Carbohydrate Polymers 83 (2011) 1–7

Contents lists available at ScienceDirect

Carbohydrate Polymers

journal homepage: www.elsevier.com/locate/carbpol

Effects of slushing process on the pore structure and crystallinity in old corrugated container cellulose fibre

Wen-Jie Guo[a,*], Yan Wang[a], Jin-Quan Wan[a,b], Yong-Wen Ma[a,**]

[a] School of Environmental Science and Engineering, South China University of Technology, Guangzhou 510006, China
[b] State Key Laboratory of Pulp and Paper Engineering, South China University of Technology, Guangzhou 510640, China

ARTICLE INFO

Article history:
Received 25 January 2010
Received in revised form 25 June 2010
Accepted 4 July 2010
Available online 13 July 2010

Keywords:
Slushing
Pore structure
Crystallinity
Cellulose
Hydrogen bond
Fractal
FTIR
Low-temperature nitrogen adsorption
OCC

ABSTRACT

Variation in the pore structure and the crystalline of old corrugated container cellulose fibre during slushing was investigated using low-temperature nitrogen adsorption, Fourier transform infrared spectroscopy and fractal geometry. With increasing slushing time, the fibre bundles decrease gradually, and become single fibre finally, meanwhile some fibres are cut off. The Brunauer–Emmett–Teller surface area of the fibres increased to 18% after 20 min comparing with 5 min, and the Barrett–Joyner–Halendar (BJH) pore volume of the fibres increased to 31% after 15 min and then to 17.5% after 20 min comparing with 5 min, but the BJH average pore size of the fibres changed little. The fractal dimensions, the crystallinity and the hydrogen bonding strength of the fibre cellulose increased first and then decreased with increasing slushing time. No new chemical group appeared during slushing. With increasing slushing time, the water retention value (WRV) of the fibres increased. The increase of WRV was due to the change of the fractal dimension and crystallinity of the fibres.

1. Introduction

With the increase of protecting the forest resources and the ecological environment, waste paper papermaking becomes an important development tendency in the world. Waste paper, as a papermaking raw material, is an important renewable resource, which not only may alleviate the shortage raw material of the papermaking and save the energy consumption, but also reduces the serious environmental pollution. In 2006, the waste paper recovery reached 196 million tons, and this year the waste paper recovery will reach 230 million tons in the world (Kuang, 2009).

Comparing with virgin plant fibre pulping, waste paper pulping could save 3 m^3 landfill, 240 kg soda ash, 75% pollutant emissions, and 40–50% energy consumption (Lu & Gao, 2009). With the increase of recycle times, the physical property of waste paper cellulose fibre decreases fast. In general, due to the decay of plant fibre quality, waste paper only reuses 3–4 times. The main reasons causing these decay is that fibre cell structure happened irreversible changes called the decay of fibre in recycling process. Latest studies from home and abroad indicate it can slowdown delay of fibre by means of chemical and physical methods, such as optimizing the process, adding agents, and so on. Therefore, it is important that the structure changes of plant fibre in recycling process are studied.

At present old corrugated container (OCC) is one of the main recycled paper, about 40% of the total waste paper. Therefore, the study focuses on OCC.

Waste paper fibres, namely recycled fibres, are porous materials. Pores exist already in native wood fibres but are also created during the pulping and bleaching processes when lignin and semicellulose are removed from the wood cell wall (Maloney & Paulapuro, 1999; Topgaard & Soderman, 2002). Pore size and pore size distributions in the fibre walls are also influenced by mechanical and chemical treatments such as beating, drying, pressing and the use of wet strength agents (Häggkvist, Li, & Ödberg, 1998). The cell wall pore structure plays a significant role in determining fibre properties, such as the capacity for fibre swelling and flexibility, the strength of paper etc (Andreasson, Forsstrom, & Wagberg, 2003; Maloney & Paulapuro, 1999). The characterization of pore size and pore size distribution is important for the understanding of fibre properties. Different methods can be used to characterize the cell wall pores. The most frequently used method is the solute exclusion technique (Böttger, Thi, & Krause, 1983; Stone & Scallan, 1967). Other techniques, such as inverse size exclusion chromatography (Aggerbrandt & Samuelsson, 1964; Berthold & Salmén, 1997), the

* Corresponding author. Tel.: +86 0 13560391612; fax: +86 020 87114970.
** Corresponding author. Tel.: +86 0 13600451025; fax: +86 020 87114970.
E-mail addresses: kwauk001@163.com (W.-J. Guo), ppywma@scut.edu.cn (Y.-W. Ma).

0144-8617/$ – see front matter © 2010 Elsevier Ltd. All rights reserved.
doi:10.1016/j.carbpol.2010.07.009

NMR relaxation method (Häggkvist et al., 1998; Li & Eriksson, 1994; Maloney, Li, Weise, & Paulapuro, 1997) and low-temperature nitrogen adsorption (Chen, Wan, & Ma, 2009; Mancosky, Lucia, & Deng, 2004; Yu, Chen, Men, & Hwang, 2009) are also available.

However, pore geometry is not easily described. Pore size, shape, surface area and connectivity all exhibit varying levels of complexity. Simplification of structure has traditionally been used to enable these geometric problems to be described in "Euclidean" terms, but the inadequacies of this approach are well known. There is strong interest surrounding the possibility of better describing these natural geometric structures. One of the new conceptual instruments at the disposition of researchers is "Fractal Geometry", which was developed during the last century but which is especially linked to its recognition and formalization in the 1970s by Mandelbrot (Atzeni, Pia, Sanna, & Spanu, 2008).

Fractal geometry allows the characterization of objects in terms of their self-similar (scale invariant) properties, i.e. parts of the object are similar to the whole after rescaling (Mandelbrot, 1982). Fractal techniques have been used in diverse engineering applications that involve physical phenomena in disordered structures and over multiple scales (Pitchumani & Ramakrishnan, 1999).

There are a lot of studies concerning pore structure related to fractal geometry (Avnir, Farin, & Pfeifer, 1983; Avnir, Farin, & Pfeifer, 1984; Farin & Avnir, 1988; Farin & Avnir, 1989; Pfeifer & Avnir, 1983). Most surfaces are fractal in nature within a limited size scale, i.e. they are characteristically self-similar upon the variation of measuring resolution. Fractal dimensions, D, that is the parameter which currently represents the geometric fractal structure, were found to be in the complete range $2 < D < 3$: low D values indicate regularity and smoothness, intermediate D values indicate irregular surfaces and D values close to 3 indicate highly irregular surface (Dobrescu, Berger, Papa, & Ionescu, 2003). As for the fractal analysis of porous pulp fibres, there is little. It is therefore necessary to develop a new fractal model for porous pulp fibres.

In this study, low-temperature nitrogen adsorption measurements were performed to investigate possible differences in the pore size and its distribution of OCC cellulose fibre samples during slushing. Using the fractal geometry, the fractal dimensions of OCC fibre samples were calculated to elaborate on the pore structure of fibre sample surfaces. In addition, Fourier transform infrared spectroscopy (FTIR) was performed to investigate possible differences of the crystallinity and hydrogen bond of the fibre cellulose. The relation of the fractal dimensions, the cellulose crystallinity and water retention value (WRV) was also discussed.

2. Materials and methods

2.1. Materials

OCC was collected from domestic marketing.

2.2. Slushing

OCC was torn into small slip with 25 mm × 25 mm, then dipped into water for 24 h. These OCC was broken to pieces in a pulper (Hydraulic Pulper, ZQS-9, Shaanxi University of Science and Technology Machinery Works, China). The concentration, time and rotation speed were 10%, 50 °C, and 300 r/min, respectively. Then shift OCC pulp into a meshwork, washing, wresting, tearing up, equipoising water. Shift the pulp into plastic bag in store.

2.3. WRV measurements

The pulp was immersed in deionized water for 24 h, and then centrifuged at 3000 r/min for 15 min at room temperature. Finally, the samples were drying to constant weight at 105 °C. Weighing up the masses of the wet pulp and the over dry pulp, WRV was calculated as follows:

$$\mathrm{WRV} = \frac{m_0 - m_1}{m_1} \times 100\%$$

where m_0 was the wet pulp mass, and m_1 was the over dry pulp mass.

2.4. Fluorescence microscope observation

When the slushing time was 5, 10, 20 min, the pulp fibre was shifted out, and then a fluorescence microscope (ECLIPSE 90i, Nikon Co., Japan) was used to observe the surface morphology change of the fibre.

2.5. Low-temperature nitrogen adsorption isotherm measurements

The wet fibre dehydration is a process particularly important for the pore structure of fibres, which contain a large proportion of water. Several methods have been proposed in the technology fibre dehydration, among them, vacuum freeze-drying is one of the most advanced dehydration methods, providing a dry production, with porous structure and little or no shrinkage (Galle, 2001; Pachulski & Ulrich, 2007; Tsami, Krokida, & Drouzas, 1999; Wang et al., 2007). All samples were freeze dried at −81.8 °C and 760 torr for 8 h using a vacuum freeze drier (4KBTXL-75, Virtis Co., USA) to remove residual water from fibres. The low-temperature nitrogen adsorption measurements were carried out using an ASAP 2020 M micropore analyzer (Micromeritics Co., USA). High-purity N_2 was used as adsorbate and the absorption–desorption of high-purity N_2 was determined at 77 K with a liquid nitrogen trap using a static volumetric method. The manufacturer's software provides values for the Brunauer–Emmett–Teller (BET) surface area, sizes of macropores, mesopores and micropores, total pore volume and average pore size of porous materials by applying the BET equation, Barret–Joyner–Halenda (BHJ) mode, Horvath–Kawazoe (H–K) mode, DFT (Density functional theory) and T-plot to the adsorption data (Passe-Coutrin, Altenor, Cossement, Jean-Marius, & Gaspard, 2008; Sing, 2001).

2.6. Determination of infrared crystallinity index

Powdered fibre and pre-ground and dried off KBr were sifted by sieve with mesh number 200. Between 3.5 and 4.0 mg fibre and 350 mg KBr, were put onto agate mortars, mixed well and porphyrize. The mixture was poured into a tabletting mould after drying at 60 °C for 4 h, to obtain completely transparent tabletting. The infrared spectra of samples were determined by vector-33 type Fourier transform infrared spectrophotometer (FTIR). The infrared crystallinity index (N.O'KI) was determined by the ratio of the bands at 1372 and 2900 cm^{-1}.

$$\mathrm{N.O'KI} = \frac{I_{1372}}{I_{2900}} \times 100\%$$

where I_{1372} is the 1372 cm^{-1} band intensity, corresponding to CH bending vibration; and I_{2900} is 2900 cm^{-1} band intensity, corresponding to CH and CH_2 bending vibration.

3. Results and discussion

3.1. Fluorescence microscope

From Fig. 1a, it is obtained that when the slushing time is 5 min, there are many bulky fibre bundles and a few single fibers; while the slushing time is 10 min, as shown in Fig. 1b, there are less fibre

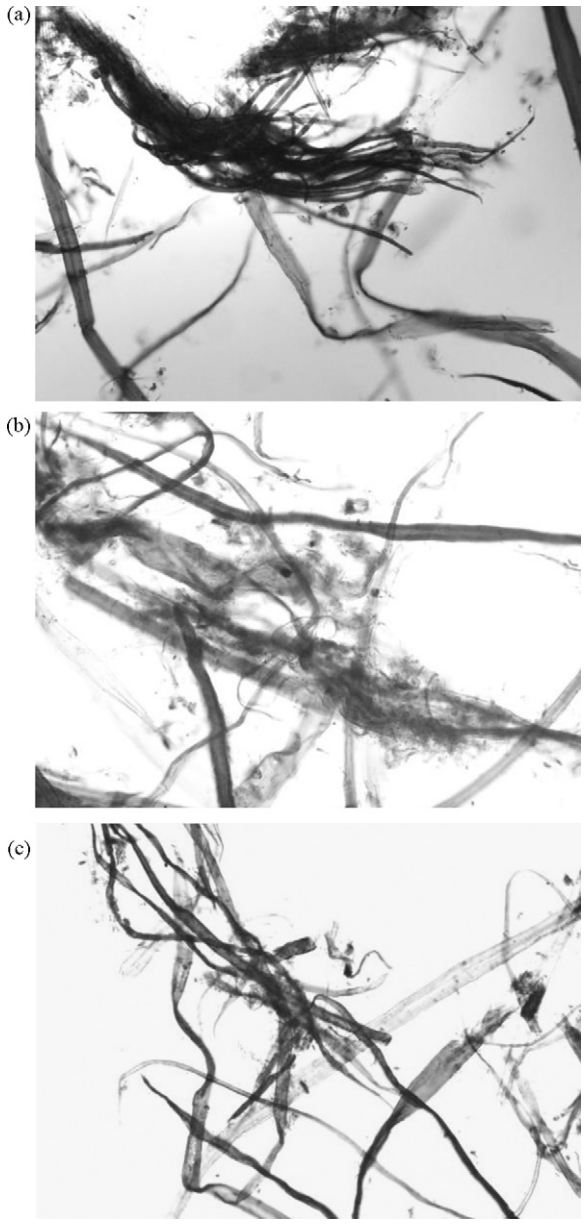

Fig. 1. Fluorescence micrograph of OCC fibre at different slushing times. (a) 5 min; (b) 10 min; (c) 20 min.

bundles and the fibre bundle volume is smaller, meanwhile the number of single fibre adds. From Fig. 1c, it is obtained that when the slushing time reaches up to 20 min, the pulp is decomposed into single fibres, and some fibres are cut off.

3.2. Low-temperature nitrogen adsorption isotherm results

The characterization of BET surface area, pore volume, pore size and pore size distributions is important for understanding fibre properties such as swelling ability and flexibility (Maloney & Paulapuro, 1999). In this study, low-temperature nitrogen adsorption method was used to investigate possible differences in the pore size and pore size distribution of fibre samples during slushing. The results of the low-temperature nitrogen adsorption measurements are given in Tables 1 and 2.

Table 1 shows that along with the increase of slushing time, the BET surface area of the fibres increased. The BET surface area of the fibre increased to 18% after 20 min comparing with 5 min.

Table 1
Pore data of OCC fibre at different slushing time.

Slushing time (min)	BET surface area ($m^2\ g^{-1}$)	BJH adsorption cumulative volume of pores ($cm^3\ g^{-1}$)	BJH adsorption average pore size (nm)
5	11.23	0.0200	5.6
10	12.10	0.0215	5.5
15	12.70	0.0262	5.7
20	13.29	0.0235	5.4

This is mainly because that the fibres were continuously wetted, and the wetted fibres produced strong friction and kneading effect in slushing process, so that the bonds between the waste paper fibres were keyed off, the impurities and thermal melting materials stripped off from the fibres (Cho, Ryu, & Song, 2009; Zhan, 1999; Zhang, Han, & Liu, 2005), this led to the increase of the BET surface area of the fibres. On the other hand, along with the increase of slushing time, the fibres could be torn, broken, and made the fibre surface producing fine fibrosis (Wu & Chen, 2006), this also resulted the increase of the surface area of the fibres.

Table 1 also shows that along with the increase of slushing time, the BJH Adsorption cumulative volume of pores first increased to 31% after 15 min comparing with 5 min, and then decreased to 17.5% after 20 min comparing with 5 min. The BJH adsorption average pore diameter changed little. This may be mainly due to changes in pore size distribution caused.

The pore size distributions of the OCC fibres were shown in Table 2.

From Tables 1 and 2, it could be seen that the pore size distribution in the OCC fibres was between 1.9 and 300 nm, and there were mainly mesopores and macropores, but there were a small amount of micropores. When the slushing time was 5 min, the volumes of the micropores, mesopores and macropores were 0.000736, 0.014724 and 0.004531 $cm^3\ g^{-1}$, respectively. When the slushing time was 15 min, the BJH adsorption cumulative volume of pores and the percentage of mesopores reached maximum, and the percentages of misopores and macropores reached the minimum. When the slushing time was 20 min, the BJH adsorption cumulative volume of pores and the percentage of mesopores decreased, and the percentages of misopores and macropores increased. These were mainly because that slushing process mainly produced misopores and mesopores, meanwhile misopores could integrate to form mesopore, and mesopores could integrate to form masopore.

3.3. Fractal characteristics of the pore in OCC fibres

Fractal Geometry describes a figure whose segments are similar to their integer (Liu, 2006). The radical characteristics of a fractal figure are self-comparability and scale-invariance. Self-comparability means that certain configurations or processes are always similar to each other at all scales or times. In other words, its part and whole properties are similar. The physical essence of this self-comparability is scale-invariance. It is this scale-invariance that means the observer can zoom in on any part in a fractal figure, and the enlarged figure will be similar to the source. So when zooming in or out of a fractal figure, its morphology, complexity and irregularity do not change. Fractals are grouped into regular fractals and irregular fractals. Regular fractals have strict self-comparability, whereas irregular fractals have only statistical self-comparability. The fractal dimension, D, is the parameter which represents the characteristic of a fractal structure.

Self-comparability can be described in mathematically as follows,

$F(x)$ expresses certain law. To all $\lambda > 0$, if,

$$F(\lambda x) = \lambda^D F(x) \quad (1)$$

Table 2
Pore size distribution of OCC fibre at different slushing time.

Pore size range (nm)	BJH adsorption incremental pore volume ($cm^3\ g^{-1}$)			
	5 min	10 min	15 min	20 min
314.2–201.2	0.001521	0.001525	0.001705	0.001530
201.2–96.2	0.001784	0.001796	0.002111	0.001814
96.2–77.1	0.001226	0.001233	0.001291	0.001241
77.1–40.0	0.001941	0.001972	0.002318	0.002014
40.0–27.1	0.001064	0.001096	0.001354	0.001140
27.1–20.6	0.000787	0.000820	0.000930	0.000865
20.6–16.6	0.000536	0.000571	0.000704	0.000617
16.6–13.9	0.000354	0.000390	0.000594	0.000437
13.9–11.7	0.000437	0.000482	0.000634	0.000540
11.7–10.5	0.000249	0.000279	0.000403	0.000319
10.5–8.4	0.000439	0.000518	0.000907	0.000623
8.4–7.0	0.000535	0.000617	0.000806	0.000726
7.0–6.0	0.000381	0.000466	0.000851	0.000579
6.0–5.2	0.000382	0.000471	0.000803	0.000588
5.2–4.1	0.001202	0.001388	0.001766	0.001636
4.1–3.0	0.001994	0.002942	0.003157	0.002688
3.0–2.0	0.004423	0.004805	0.005221	0.005316
2.0–1.9	0.000736	0.000771	0.000622	0.000818

this law is called self-comparability, where D is a constant, namely fractal dimension.

As regards a practical fractal figure, its self-comparability is not strict, and in general, it belongs to irregular fractal. It also is of self-comparability in some range.

Katz and Thompson (1985) analyzed the geometric structure of pore materials. Their study showed that both the pore spaces and surfaces were fractal, and that their fractal dimensions were equal. The fractal dimension could be applied to forecast the void fraction of a pore material. Friesen et al, also showed that a pore material was fractal if its pore size was in the range of 1 nm to 1 μm, and the roughness and complexity of the fractal dimension of a pore material could be quantified (Coppens & Froment, 1995; Friesen & Mikula, 1987; Leon, 1998). If the fractal dimension of a pore material is between 2 and 3, the larger the value of D is, the more complex the pore structure is.

The majority of actual figures, do not exhibit strict self-comparability, and are hence irregular fractals. Such figures may, however, exhibit self-comparability in certain ranges. Yu (2003) had also given a criterion which decided whether a porous material was fractal, namely,

$$\left(\frac{\lambda_{\min}}{\lambda_{\max}}\right)^{D_f} = 0 \tag{2}$$

where $\lambda_{\min}$ and $\lambda_{\max}$ were the minimum and maximum values of the pore size of a porous material; D_f was the fractal dimension of the material. Meanwhile, D_f was between 2 and 3 to three dimensional space.

From a fractal geometry based interpretation of the pore structure of a fibre, the pore size, r, and the number of pores, $N(>r)$, of size greater r, has the following relation:

$$N(>r) = \int_{r}^{r_{\max}} f(r)\ dr = k_0 r^{-D} \tag{3}$$

where $r_{\max}$ is the largest pore size in a cellulose fibre, $f(r)$is the pore size function, k_0 is a constant, and D is the fractal dimension of a cellulose fibre.

Eq. (2) may be written as

$$f(r) = \frac{dN(>r)}{dr} = k_1 r^{-1-D} \tag{4}$$

where k_1 is a constant, and equals $-Dk_0$.

The cumulative pore volume, $V(<r)$, which pore radius is less than r, is

$$V(<r) = \int_{r_{\min}}^{r} f(r) c r^3\ dr \tag{5}$$

where c is a constant.

From Eqs. (4) and (5), the cumulative volume $V(<r)$ of pores sized less than r, can be derived:

$$V(<r) = k_2(r^{3-D} - r_{\min}^{3-D}) \tag{6}$$

where k_2 is a constant, and equals $ck_1/(3-D)$.

In the same way, the overall pore volume of a cellulose fibre is

$$V = k_2(r_{\max}^{3-D} - r_{\min}^{3-D}) \tag{7}$$

S is the cumulative volume fraction with pore size less than r, and S can be given by

$$S = \frac{V(r)}{V} = \frac{r^{3-D} - r_{\min}^{3-D}}{r_{\max}^{3-D} - r_{\min}^{3-D}} \tag{8}$$

Considering $r_{\min} \ll r_{\max}$, Eq. (8) can be rewritten as

$$S = \left(\frac{r}{r_{\max}}\right)^{3-D} \tag{9}$$

$$\ln S = (3-D)\ \ln r + K \tag{10}$$

where K is a constant, and equals $-(3-D)\ln r_{\max}$.

As for pulp fibre, it is a porous material, with a pore size between 1 and 500 nm, and $r_{\min}/r_{\max}$ is very small, approximately equals to 0.01, therefore we can approximatively regard $(r_{\min}/r_{\max})^{D_f}$ as 0. We can determine the relation between the pore volume and the pore size of pulp fibre by means of certain method, calculate $\ln S$, and then draw out the curve of $\ln S$ versus $\ln r$. If the curve is linear, the slope of the curve is $3-D$, and D is between 2 and 3, this indicates the pore structure of pulp fibre meets scale-invariance, so we can regard the pore structure of pulp fibre as a fractal, and D is the fractal dimension of pulp fibre.

According to Table 2, S is worked out; the curves of $\ln S$ versus $\ln r$ are shown in Figs. 2–5.

From Figs. 2–5, it is obtained that the curves of $\ln S$ versus $\ln r$ are linear in some range, namely *bc* segment (the pore size is approximately 5–350 nm) in the figures. Therefore, we can regard a OCC fibre as a fractal figure in this range. In the smaller pore size range, namely *ab* segment (the pore size is smaller than 5 nm) in the figures, there is biggish negative deviation. This is mainly because that

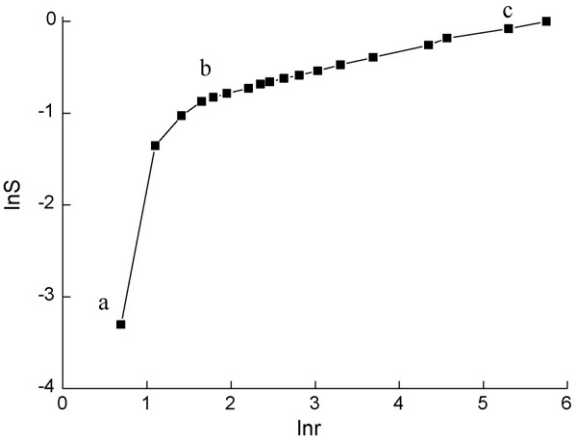

Fig. 2. ln *S* versus ln *r* (slushing time 5 min).

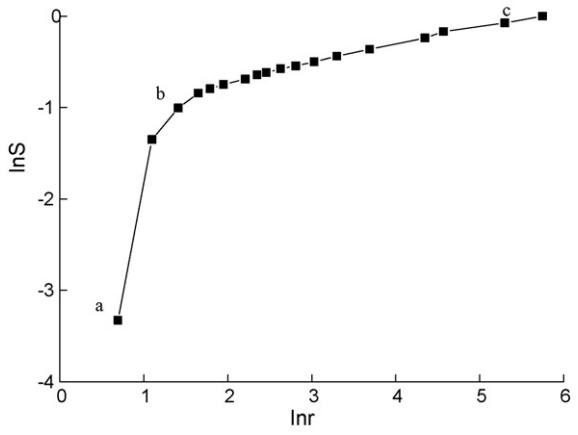

Fig. 3. ln *S* versus ln *r* (slushing time 10 min).

the micropore analyzer actual survey's lower limit approximately is 1.9 nm, so the fine pore is unable to be measured correctly. On the other hand there possibly still is some moisture in the cellulose fibre.

According to Figs. 2–5 and Eq. (10), the fractal dimensions *D* of the fibres can be calculated, as shown in Table 3.

The fractal dimension quantificationally represents the surface morphology of a pore material. The fractal dimension, *D*, of a porous surface is between 2 and 3. The smaller *D* is, the less irregular the surface is, vice versa.

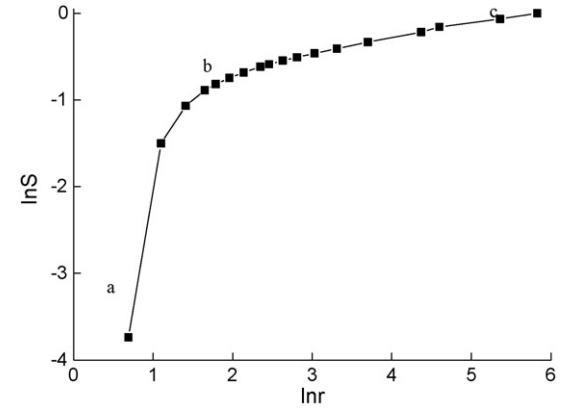

Fig. 4. ln *S* versus ln *r* (slushing time 15 min).

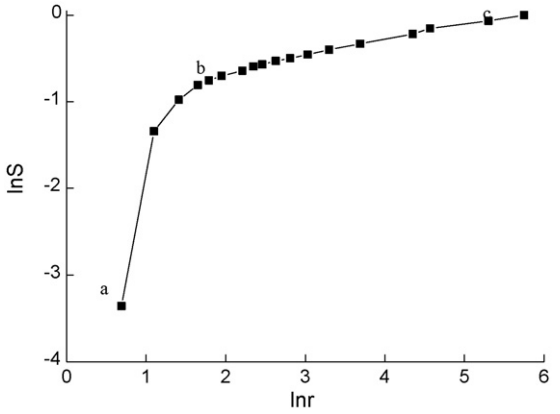

Fig. 5. ln *S* versus ln *r* (slushing time 20 min).

As shown in Table 3, along with the increase of slushing time, *D* of the OCC fibres increased significantly. When the slushing time was 15 min, *D* of the OCC fibres increased to maximum, followed by the down.

Pores exist already in native wood fibres but are also created during the slushing process because of friction and kneading effect, meanwhile misopores could integrate to form mesopores, and mesopores could integrate to form masopores. So the pore sizes and the pore size distributions in the fibre walls are influenced by slushing. In the first slushing process, the pore size became more irregular because the fibres could be torn, broken, and many new misopores and mesopores appeared, so *D* increased. But along with the slushing time added, misopores could integrate to form mesopores and mesopores could integrate to form masopores, this resulted the pore size distribution became more regular, thus the fractal dimension decreases.

3.4. Effect of slushing on the chemical bond in the fibre surface

Plant fibre is mainly composed of cellulose, hemicellulose and lignin, and cellulose is the main component, forming the skeleton of plant fibre. Cellulose is a polysaccharide which is made of many D-pyran glucoses connected by 1,4-β glycoside bond. The studies of natural cellulose supramolecular structure have shown that cellulose is made up of crystalline zone and non-crystalline zone in an interlaced form. Most hydroxyl groups of glucose is at free stage in non-crystalline zone, and many hydroxyl groups of glucose form hydrogen bonds each other in crystalline zone, these hydrogen bonds lead the formation of a dense crystal structure of cellulose. Because the amount of hydrogen bonds in cellulose crystalline zone is huge, the hydrogen bonds could determine many characteristics of cellulose, such as crystalline, water absorption, accessibility and chemical activity and so on (Nishiyama, Langan, & Chanzy, 2002; Qian, Ding, Nimlos, Johnson, & Himmel, 2005).

Fig. 6 showed that FTIR curves were analogous, and this indicated that no new functional groups came up being after slushing

Table 3
WRV, N.O'KI and *D* of OCC fibre at different slushing time.

Slushing time (min)	WRV (%)	N.O'KI (%)	*D*
5	105	105	2.786
10	108	109	2.796
15	112	108	2.811
20	117	106	2.807

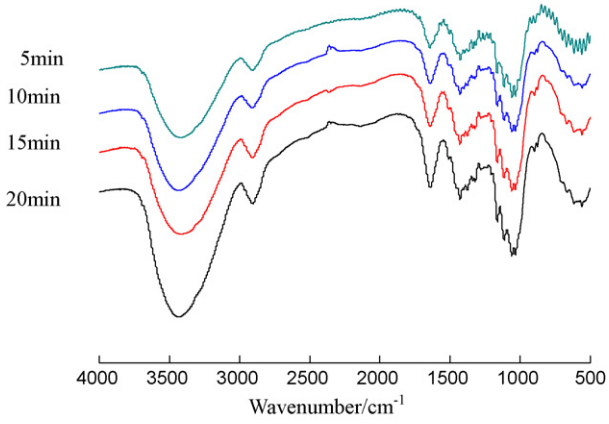

Fig. 6. FTIR spectra of OCC fibre at different slushing time.

process. The absorption peak of the hydrogen bond stretching vibration frequency was at 3372 cm^{-1}. When the slushing time was from 5 min up to 10 min, the absorption peak slightly increased, which suggested that there was the increase of the hydrogen bond strength after slishing. When the slushing time was up to 15 min, the absorption peak markedly decreased, which suggested that there was a drop of the hydrogen bond strength.

3.5. The relation of the fractal dimension, the crystallinity and WRV of OCC fibre

The fractal dimension and crystallinity of a pulp fibre have important impact on WRV. The relationship between *D*, N.O'KI and WRV is shown in Table 3. The crystallinity of cellulose is, to some extent, a reflection of the physical and chemical performances of cellulose. In general, with the increase of crystallinity, fibre' tensile strength, hardness, relative density and dimensional stability are improved, but its softness, chemical activity are reduced. Therefore, the measurements of the cellulose' crystallinity are important to understand the cellulose' nature.

As shown in Table 3, along with the increase of slushing time, N.O'KI of cellulose first increased slightly, and then reduced. This was mainly due that slushing mainly acted on the amorphous area in first, and then on the crystalline zone. This led that N.O'KI of cellulose begun to fall after 15 min.

From Table 3, it can be seen that slushing had important impact on WRV. Along with the increase of slushing time, WRV increased. This was due that WRV was decided by the fractal dimension and the crystallinity of OCC fibre. When the slushing time was less than 10 min, the increase of WRV was mainly due to the increase of the fractal dimension. When the slushing time was more than 15 min, the increase of WRV was mainly due to the decrease of the OCC fibre crystallinity.

4. Conclusions

Along with the increase of slushing time, the fibre bundles decrease gradually, and become single fibre finally, meanwhile some fibres are cut off.

Along with the increase of slushing time, the BET surface area of OCC fibre significantly increased. The cumulative pore volume increased first and then decreased, while the average pore size change was very small.

Fractal geometry analysis of the results showed that the fractal dimensions increased in first, and then decreased along with the increase of slushing time.

FTIR analysis of the results showed that no new functional group was generated after slushing process, and the hydrogen bond strength increased first and then decreased along with the increase of slushing time.

The crystallinity of cellulose first increased slightly, and then reduced along with the increase of slushing time.

WRV increased along with the increase of slushing time. The increase of WRV was mainly due to the decrease of the crystallinity and the increase of the fractal dimension of the OCC fibre.

Acknowledgements

This work was supported by a grant from by the National High Technology Research and Development Program of China (No. 2007AA03Z433) and Natural Science Youth Fund Project of South China University of Technology. We thank the School of Environmental Science and Engineering, South China University of Technology for the use of the micropore analyzer.

References

Aggerbrandt, L. G., & Samuelsson, O. (1964). Penetration of water-soluble polymers into cellulose fibres. *Journal of Applied Polymer Science*, *8*, 2801–2812.
Andreasson, B., Forsstrom, J., & Wagberg, L. (2003). The porous structure of pulp fibres with different yields and influence on paper strength. *Cellulose*, *10*, 111–123.
Atzeni, C., Pia, G., Sanna, U., & Spanu, N. (2008). A fractal model of the porous microstructure of earth-based materials. *Construction and Building Materials*, *22*(8), 1607–1613.
Avnir, D., Farin, D., & Pfeifer, P. (1983). Chemistry in noninteger dimensions between two and three. II. Fractal surfaces of adsorbents. *Journal of Chemical Physics*, *79*(7), 3566–3571.
Avnir, D., Farin, D., & Pfeifer, P. (1984). Molecular fractal surfaces. *Nature*, *308*(5956), 261–263.
Berthold, J., & Salmén, L. (1997). Inverse size exclusion chromatography (ISEC) for determing the relative pore size distribution of wood pulps. *Holzforschung*, *51*(4), 361–368.
Böttger, J., Thi, L., & Krause, T. (1983). Untersuchungen zur Porenstruktur von Zellstoffasern. *Das Papier*, *37*(10A), V14–V21.
Chen, Y. M., Wan, J. Q., & Ma, Y. W. (2009). Effect of noncellulosic constituents on physical properties and pore structure of recycled fibre. *APPITA Journal*, *62*(4), 290–302.
Cho, B. U., Ryu, J. Y., & Song, B. K. (2009). Factors influencing deflaking kinetics in repulping to produce molded pulp. *Journal of Industrial and Engineering Chemistry*, *15*, 119–123.
Coppens, M. O., & Froment, G. F. (1995). Knudsen diffusion in porous catalysts with a fractal internal surface. *Fractals*, *3*(4), 807–820.
Dobrescu, G., Berger, D., Papa, F., & Ionescu, N. I. (2003). Fractal dimensions of lanthanum ferrite samples by adsorption isotherm method. *Applied Surface Science*, *220*(1–4), 154–158.
Farin, D., & Avnir, D. (1988). In K. K. Unger, D. Behrens, & H. Kral (Eds.), *Characterization of porous solids* (p. 421). Amsterdam: Elsevier.
Farin, D., & Avnir, D. (1989). In D. Avnir (Ed.), *The fractal approach to heterogeneous chemistry: Surfaces, colloids, polymers* (p. 271). Chichester: Wiley.
Friesen, W. I., & Mikula, R. J. (1987). Fractal dimensions of coal particles. *Journal of Colloid and Interface Science*, *120*(1), 263–271.
Galle, C. (2001). Effect of drying on cement-based materials pore structure as identified by mercury intrusion porosimetry—A comparative study between oven-, vacuum-, and freeze-drying. *Cement and Concrete Research*, *31*, 1467–1477.
Häggkvist, M., Li, T. Q., & Ödberg, L. (1998). Effects of drying and pressing on the pore structure in the cellulose fibre wall studied by ^{1}H and ^{2}H NMR relaxation. *Cellulose*, *5*, 33–49.
Katz, A. J., & Thompson, A. H. (1985). Fractal sandstone pores: Implications for conductivity and pore formation. *Physical Review Letters*, *54*(12), 1325–1328.
Kuang, S. J. (2009). Overview of the global paper industry in 2008. *China Paper Newsletter*, *11*, 13–15 (in Chinese).
Leon, C. A. L. Y. (1998). New perspectives in mercury porosimetry. *Advances in Colloid and Interface Science*, *76–77*, 341–372.
Li, T. Q., & Eriksson, U. (1994). Kaolin-based coating layer studied by ^{2}H and ^{1}H NMR relaxation method. *Langmuir*, *10*, 4624–4629.
Liu, D. J. (2006). *Fractal theory application in chemical engineering*. Beijing: Chemical Industry Press. (in Chinese).
Lu, Z. H., & Gao, Y. J. (2009). Prospect of waste paper regeneration. *Tianjin Paper Making*, *4*, 26–28 (in Chinese).
Maloney, T. C., Li, T. Q., Weise, U., & Paulapuro, H. (1997). Intra- and inter-fibre pore closure in wet pressing. *Appita Journal*, *50*(4), 301–306.
Maloney, T. C., & Paulapuro, H. (1999). The formation of pores in the cell wall. *Journal of Pulp and Paper Science*, *25*(12), 430–436.

Mancosky, D. G., Lucia, L. A., & Deng, Y. L. (2004). The effects of lignocellulosic fiber surface area on the dynamics of lignin oxidation and diffusion. *Journal of Applied Polymer Science*, *94*(1), 177–181.

Mandelbrot, B. B. (1982). *The fractal geometry of nature*. New York: Freeman., p. 23.

Nishiyama, Y., Langan, P., & Chanzy, H. (2002). Crystal structure and hydrogen bonding system in cellulose I_β from synchrotron X-ray and neutron fiber diffraction. *Journal of the America Chemical Society*, *124*(31), 9074–9082.

Pachulski, N., & Ulrich, J. (2007). New fields of application for sol–gel process cold and vacuum-free 'compacting' of pharmaceutical materials to tablets. *Chemical Engineering Research and Design*, *85*(A7), 1013–1019.

Passe-Coutrin, N., Altenor, S., Cossement, D., Jean-Marius, C., & Gaspard, S. (2008). Comparison of parameters calculated from the BET and Freundlich isotherms obtained by nitrogen adsorption on activated carbons: A new method for calculating the specific surface area. *Microporous and Mesoporous Materials*, *111*(1–3), 517–522.

Pfeifer, P., & Avnir, D. (1983). Chemistry in noninteger dimensions between two and three. I. fractal theory of heterogeneous surface. *Journal of Chemical Physics*, *79*(7), 3558–3565.

Pitchumani, R., & Ramakrishnan, B. (1999). A fractal geometry model for evaluating permeabilities of porous performs used in liquid composite molding. *International Journal Heat and Mass Transfer*, *42*(12), 2219–2232.

Qian, X. H., Ding, S. Y., Nimlos, M. R., Johnson, D. K., & Himmel, M. E. (2005). Atomic and electronic structures of molecular crystalline cellulose I_β: A first-principles investigation. *Macromolecules*, *38*, 10580–10589.

Sing, K. (2001). The use of nitrogen adsorption for the characterisation of porous materials. *Colloids and Surfaces A: Physicochemical and Engineering Aspects*, *187*(31), 3–9.

Stone, J. E., & Scallan, A. M. (1967). The effect of component removal upon the porous structure of the cell wall of wood. II. Swelling in water and the fiber saturation point. *Tappi Journal*, *50*, 496–501.

Topgaard, D., & Soderman, O. (2002). Changes of cellulose fiber wall structure during drying investigated using NMR self diffusion and relaxation experiments. *Cellulose*, *9*, 139–147.

Tsami, E., Krokida, M. K., & Drouzas, A. E. (1999). Effect of drying method on the sorption characteristics of model fruit powders. *Journal of Food Engineering*, *38*(4), 381–392.

Wang, Y. L., Du, B. Y., Liu, J., Lu, J., Shi, B. Y., & Tang, H. X. (2007). Surface analysis of cryofixation-vacuum-freeze-dried polyaluminum chloride–humic acid (PACl–HA) flocs. *Journal of Colloid and Interface Science*, *316*, 457–466.

Wu, M., & Chen, K. F. (2006). Design of high consisitency pulper used in laboratory. *Paper and Paper Making*, *25*(1), 38–41 (in Chinese).

Yu, B. M. (2003). Advances of fractal analysis of transport properties for porous media. *Advances in Mechanics*, *33*(3), 333–346 (in Chinese).

Yu, C. T., Chen, W. H., Men, L. C., & Hwang, W. S. (2009). Microscopic structure features changes of rice straw treated by boiled acid solution. *Industrial Crops and Products*, *29*, 308–315.

Zhan, H. Y. (1999). Waste paper recycling technology lectures: Defibering and beating of waste paper and waste of dissociation beating recycle waste paper technology lectures. *Guangdong Pulp and Paper*, *2*, 43–51 (in Chinese).

Zhang, S. J., Han, Q., & Liu, H. B. (2005). Effect of the equipment factor to fiber quality duringwaster paper recycling. *Journal of Shaanxi University of Science and Technology (Natural Science Edition)*, *23*(2), 12–16 (in Chinese).